

# The diocotron instability in a pulsar “cylindrical” electrosphere.

Jérôme Pétri<sup>1</sup>

Max-Planck-Institut für Kernphysik, Saupfercheckweg 1, 69117 Heidelberg, Germany.

Received / Accepted nov. 2006

## ABSTRACT

*Context.* The physics of the pulsar inner magnetosphere remains poorly constrained by observations. Although about 2000 pulsars have been discovered to date, little is known about their emission mechanism. Large vacuum gaps probably exist and a non-neutral plasma made of electrons in some regions and of positrons in some other regions fills space to form an electrosphere.

*Aims.* The purpose of this work is to study the stability properties of the differentially rotating equatorial disk in the pulsar’s electrosphere for which the magnetic field is assumed to be dipolar. In contrast to previous studies, the magnetic field is not restricted to be uniform.

*Methods.* A pseudo-spectral Galerkin method using Tchebyshev polynomials expansion is developed to compute the spectrum of the diocotron instability in a non-neutral plasma column confined between two cylindrically conducting walls. Moreover, the inner wall carries a given charge per unit length in order to account for the presence of a charged neutron star at the centre of the electrosphere.

*Results.* We show several eigenfunctions and eigenspectra obtained for different initial density profiles and electromagnetic field configurations useful for laboratory plasmas. The algorithm is very efficient in computing the fastest growing modes. Applications to a “cylindrical” electrosphere are also shown for several differential rotation profiles. It is found that the growth rates of the diocotron instability are of the same order of magnitude as the rotation rate.

*Conclusions.* The instability develops on a very short timescale and can account for very efficient particle diffusion across the magnetic field lines as already claimed in a previous work. The exact geometry of the confined plasma, let it be a thin disk or a cylinder, does not significantly affect the spectrum of the diocotron instability.

**Key words.** Instabilities – Methods: analytical – Methods: numerical – Stars: neutron

## 1. INTRODUCTION

The detailed structure of charge distribution and electric current circulation in the closed magnetosphere of a pulsar remains poorly understood. Although it is often assumed that the plasma entirely fills the space and corotates with the neutron star, it is on the contrary very likely that it only partly fills it, leaving large vacuum gaps in between plasma-filled regions. The existence of such gaps in aligned rotators has been very clearly established by Krause-Polstorff and Michel (1985a, 1985b).

Since then, a number of different numerical approaches to the problem have confirmed their conclusions, including some work by Rylov (1989), Shibata (1989), Zachariades (1993), Neukirch (1993), Thielheim and Wolfst  ller (1994), Spitkovsky and Arons (2002) and by ourselves (P  tri et al. 2002a). This conclusion on the existence of vacuum gaps has been reached from a self consistent solution of Maxwell’s equations in the case of the aligned rotator. Moreover, Smith et al. (2001) have shown by numerical modeling that an initially filled magnetosphere like the Goldreich-Julian model evolves by opening up large gaps and stabilises to the partially filled and partially void solution found by Krause-Polstorff and Michel (1985a) and also by P  tri et al. (2002a). The status of models of the pulsar magnetospheres, or electrospheres, has been recently critically reviewed by Michel (2005). A solution with vacuum gaps has the peculiar property that those parts of the magnetosphere which are separated (following magnetic field lines) from the star’s surface by a vacuum region are not corotating and suffer differential rotation.

This rises the question of the stability of such charged plasma flow. The differential rotation in the equatorial non neutral disk induces the so-called diocotron and magnetron instabilities, well known to plasma physicists (O’Neil 1980, Davidson 1990, O’Neil and Smith 1992). In the inner parts of the magnetosphere, far from the light cylinder, the instability reduces to its electrostatic form, the diocotron instability. The linear development of the diocotron instability of a thin differentially rotating charged disk has been studied by P  tri et al (2002b) and shown to proceed at a growth rate comparable to the star’s rotation rate. The non linear development of this instability has been studied by P  tri et al (2003), still in the framework of an infinitely thin disk model. When there is no external source of charges feeding the magnetosphere, it has been found that the plasma remains confined in regions close to the equilibrium state as also shown by Aly (2005). When however the disk can be fed by some charge source, P  tri et al (2003) have shown that the instability causes a cross-field transport of these charges in the equatorial disk, evolving into a net out-flowing flux of charges. Spitkovsky and Arons (2002) have numerically studied the problem, and concluded that such charge transport tends to fill the gaps with plasma. Since a filled magnetosphere is stable to the diocotron instability, it seems unlikely that the instability could indeed bring the system to a completely filled state, even though the disk would not remain thin, as assumed by P  tri et al. (2002b, 2003). It should be noted that the appearance of a cross-field electric current as a result of the diocotron instability has been observed by Pasquini and Fajans (2002) in laboratory experiments in which charged particles were continuously injected in the plasma column trapped in a Malmberg-Penning configuration.

The aim of this work is to show that the fact that the differentially rotating charged disk is not infinitely thin does not invalidate our former conclusion (P  tri et al. 2002a) that the growth rate of the instability is as fast as the star’s rotation rate. The situation opposite to a thin disk is that of an infinitely thick disk. By this we mean a plasma column, the structure of which is invariant with the cylindrical coordinate  $z$  and in which the magnetic field is dependent on the cylindrical coordinate  $r$  and oriented parallel to the  $z$  direction. Whereas the thin disk model can conveniently describe perturbations the horizontal size of which is much larger than the disk’s thickness, the (infinitely) thick model would be more appropriate to perturbations the horizontal size of which is much less than the disk’s thickness. In the electrostatic approximation the magnetic field is not altered by the perturbations and remains straight. From the inertia-less approximation, the charged fluid velocity is given by eq. (17) which implies that  $\mathbf{E} + \mathbf{v} \times \mathbf{B} = 0$  and then that  $\mathbf{E} \cdot \mathbf{B} = 0$ . As a result the perturbed

electric field and flow are 2-dimensional, since the electric potential perturbation is independent of  $z$ . It should be kept in mind that the infinitely thick disk model with a  $z$ -aligned magnetic field is in fact meant to represent a disk of a finite thickness embedded in a 2D potential magnetic field. Such 2D fields, like

$$\mathbf{B} = B_r(r, z)\mathbf{e}_r + B_z(r, z)\mathbf{e}_z \quad (1)$$

as opposed to 1D fields like  $\mathbf{B} = B_z(r)\mathbf{e}_z$ , may be current free and still have a radial dependence of  $B_z(r, 0)$  in the equatorial plane. In the 1D model, the disk, though not infinitely thin, is regarded as not being thick enough for the radial field component  $B_r(r, z)$  to play a role. The component  $B_z(r, 0)$  is taken as an approximation to  $B_z(r, z)$ . The domain of validity of a 1D model then is that  $B_r(r, z)$  remains small in the disk, while the horizontal size of the perturbations is less than the disk’s thickness. The real situation is in between the infinitely thin and the infinitely thick disk model. Dealing with a finite thickness disk would involve the consideration of the 2D magnetic field structure and the numerical calculation of the solution to the Poisson’s equation in the appropriate geometry. Obtaining this solution has been the most time consuming part of the calculations in P  tri et al. (2003) and things would be even worse if a 2D geometry with a thick disk were to be considered. Adopting a 1D unperturbed geometry model considerably alleviates such difficulties and seems appropriate to reach a conclusion on the range in which the growth rates of the diocotron instability are to be found when the infinitely thin disk approximation is relaxed.

In this paper we present a numerical analysis of the linear growth of the diocotron instability in the 1D model. We plan to compute the full non linear development of the instability in the same geometry, by using a 2D electrostatic PIC code, a study that would also be relevant to laboratory setups.

The diocotron spectrum for cylindrical geometry and uniform external magnetic field has been investigated analytically by Levy (1965) and numerically by Goswami et al. (1999) who used a finite difference schemes. Variational techniques for toroidal non-neutral plasmas have also been used, see Bhattacharyya (2000).

The paper is organized as follows. In Sec. 2, we describe the initial setup of the plasma column in the laboratory consisting of an axially symmetric equilibrium between two conducting walls. The slightly different approach used for the pulsar’s electrosphere is also described. In Sec. 3, we recall the generalised linear eigenvalue problem satisfied by the perturbed electric potential. Next, in Sec. 4, the pseudo-spectral Galerkin numerical algorithm to compute the diocotron spectrum is presented. Finally, some typical spectra for laboratory plasma are shown in Sec. 5. We discuss in more detail the application to electrospheric plasmas which is the main aim of this work. The conclusions and the possible generalisation are presented in Sec. 6.

## 2. INITIAL SETUP

In laboratory plasmas, the motion of particles is imposed by external devices controlling the potential and electric field. It is the most common situation. However, having in mind to applied the algorithm to pulsar’s electrosphere, it is also interesting to study the stability properties of non-neutral plasmas by imposing the rotation profile instead of the density profile. Therefore, we first describe the case encountered in the laboratory and then discussed how to apply and extend it to pulsars.

### 2.1. Laboratory plasma

We consider a one species non-neutral plasma consisting of particles with mass  $m$  and charge  $q$  trapped between two cylindrically conducting walls located at  $r = W_1$  and  $r = W_2 > W_1$ . The plasma column itself is confined between  $R_1 \geq W_1$  and  $R_2 \leq W_2$ . This allows us to take into account vacuum regions between the plasma and the conducting walls. We adopt cylindrical coordinates denoted by  $(r, \varphi, z)$  and the corresponding basis vectors  $(\mathbf{e}_r, \mathbf{e}_\varphi, \mathbf{e}_z)$ . In order to simulate the presence of a charged neutron star generating a radial electric field, the inner wall at  $W_1$  carries a charge  $Q$  per unit length such that its electric field is simply given by Maxwell-Gauss theorem :

$$\mathbf{E}_w(r) = \frac{Q}{2\pi\epsilon_0 r} \mathbf{e}_r \quad (2)$$

In the equilibrium configuration, the particle number density is  $n(r)$  and the charge density is  $\rho(r) = q n(r)$ . In contrast to earlier studies, the external magnetic field, along the  $z$ -axis, is not necessarily uniform

$$\mathbf{B} = B_z(r) \mathbf{e}_z \quad (3)$$

Strictly speaking, this magnetic field is associated with an azimuthal current because  $\nabla \wedge \mathbf{B} \neq \mathbf{0}$ . However, as claimed in the introduction, there is also a (weak) radial component Eq. (1) which should compensate for this current. Let’s find the conditions for which approximation Eq. (3) holds, assuming a power law for  $B_z$ , Eq. (48). From Eq. (1), the  $\varphi$ -component of the curl reads

$$\frac{\partial B_r}{\partial z} - \frac{\partial B_z}{\partial r} = \frac{\partial B_r}{\partial z} + \alpha \frac{B_z}{r} \quad (4)$$

With the boundary conditions  $B_r(r, z = 0) = 0$ , we found that near the equatorial plane

$$B_r = -\alpha \frac{z}{r} B_z \quad (5)$$

$\alpha$  being of order unity, the radial component of the magnetic field is negligible whenever  $z \ll r$ . Therefore, our approximation Eq. (3) holds in the thin disk limit (intermediate between infinitely thin and infinitely thick).

The electric field is made of two parts, the first one arising from the plasma column  $\mathbf{E}_p$  itself, and the second one from the inner conducting wall  $\mathbf{E}_w$ , Eq. (2). We assume that the electric field induced by the plasma vanishes at  $r = W_1$ , i.e.  $\mathbf{E}_p(W_1) = \mathbf{0}$ . We therefore get

$$\mathbf{E}_p(r) = \frac{1}{\epsilon_0 r} \int_{W_1}^r \rho(r') r' dr' \mathbf{e}_r \quad (6)$$

The total electric field, directed along the radial direction  $\mathbf{e}_r$ , is therefore

$$\mathbf{E} = \mathbf{E}_p + \mathbf{E}_w = E_r \mathbf{e}_r \quad (7)$$

At equilibrium, the plasma is rotating between the two walls at a speed  $\Omega(r)$ . The particles have mass  $m_e$  and charge  $q$ . In the stationary state, the centrifugal force is balanced by the Lorentz force such that

$$q(E_r + r\Omega B_z) + m_e r\Omega^2 = 0 \quad (8)$$

Introducing the cyclotron frequency by  $\omega_c = \frac{qB_z}{m_e}$  and the plasma frequency by  $\omega_p^2 = \frac{nq^2}{m_e \epsilon_0}$ , the angular speed of the column satisfies the quadratic equation

$$\Omega^2 + \omega_c \Omega + \frac{qE_r}{m_e r} = 0 \quad (9)$$

leading to two possible solutions for  $\Omega$ , namely

$$\Omega = -\frac{\omega_c}{2} \left[ 1 \pm \sqrt{1 - 4 \frac{q E_r}{m_e r \omega_c^2}} \right] \quad (10)$$

If the electric field is sufficiently weak, i.e.  $q E_r \ll m_e r \omega_c^2$ , the solutions are approximated by  $\Omega = -\omega_c$  and

$$\Omega = -\frac{E_r}{r B_z} \quad (11)$$

The weak field limit is equivalent to a low density plasma column because it implies  $\omega_p^2 \ll \omega_c^2$ . The solution Eq. (11) corresponds to the usual electric drift approximation (Davidson and Tsang 1984). In the remaining of this paper, we retain this assumption. Therefore, the equation of motion for the charged particles is replaced by the electric drift approximation. Indeed, we consider only the low-density non-neutral plasma case for which the diocotron regime is valid. Neglecting electron inertia, the electric drift approximation applies. For  $Q = 0$  and a constant density profile in the plasma column with  $W_1 = 0$ , it corresponds to a circular motion at the diocotron frequency defined by, see for instance Davidson (1990)

$$\omega_D = \frac{\omega_p^2}{2 \omega_c} \quad (12)$$

## 2.2. Electrospheric plasma

Our purpose is to study the non-neutral plasma instabilities occurring in the pulsar inner magnetosphere. The most interesting feature obtained in the work by Pétri et al. (2002a) by constructing an electrospheric model was a differential rotation in the positively charged equatorial disk. It can indeed be shown that large vacuum gaps imply a significant departure from corotation. That is why when applying our algorithm to pulsars, it is more appropriate to assume a given rotation profile in the plasma  $\Omega(r)$ , instead of densities and potential imposed by external devices. In the electric drift approximation, using Maxwell-Gauss law, the charge density is recovered according to ideal MHD by

$$\mathbf{E} = -(\boldsymbol{\Omega} \wedge \mathbf{r}) \wedge \mathbf{B} \quad (13)$$

leading to the charge density as follows

$$\rho = -\varepsilon_0 \left[ \frac{B_z}{r} \frac{\partial}{\partial r} (r^2 \Omega) + r \Omega \frac{\partial B_z}{\partial r} \right] \quad (14)$$

Therefore, there are only 2 independent functions, namely the couple  $(B_z, \Omega)$  appropriate for pulsar electrospheric plasmas and the couple  $(B_z, \rho)$  useful for laboratory plasmas.

## 3. LINEAR ANALYSIS

We consider two different plasma configurations. In the first case, the plasma column is supposed to be in contact with both the inner and the outer wall. This will be called single domain. In the second case, vacuum regions exist between the plasma column and the inner and/or the outer walls. This will be called multi-domain. We introduced these two situations because of the slightly different numerical treatment of the problem. Indeed, vacuum regions are treated analytically whereas regions filled with plasma are treated numerically.

### 3.1. Single domain

Let’s start with a column density in contact with the inner and the outer conducting wall. The motion of the column of plasma is governed by the conservation of charge, the Maxwell-Poisson equation and the electric drift approximation, respectively :

$$\frac{\partial \rho}{\partial t} + \text{div}(\rho \mathbf{v}) = 0 \quad (15)$$

$$\Delta \phi + \frac{\rho}{\varepsilon_0} = 0 \quad (16)$$

$$\mathbf{v} = \frac{\mathbf{E} \wedge \mathbf{B}}{B^2} \quad (17)$$

$$\mathbf{E} = -\nabla \phi \quad (18)$$

We recall that the magnetic field remains constant in time in the diocotron regime. We apply the standard linear perturbation theory. Introducing perturbations of physical quantities  $X$  like electric potential, density and velocity components, by the expansion

$$X(r, \varphi, t) = X(r) e^{i(m\varphi - \omega t)} \quad (19)$$

the eigenvalue problem for the perturbed electric potential  $\phi(r)$  is expressed as

$$\left[ \frac{1}{r} \frac{\partial}{\partial r} \left( r \frac{\partial \phi}{\partial r} \right) - \frac{m^2}{r^2} \right] \phi = \frac{m}{(\omega - m\Omega)} \frac{1}{\varepsilon_0 r} \frac{\partial}{\partial r} \left( \frac{\rho}{B_z} \right) \phi \quad (20)$$

For the purpose of our numerical algorithm, it is more convenient to rewrite it as a generalised linear eigenvalue problem as follows

$$\omega \mathcal{L}_m(\phi) = m\Omega \mathcal{L}_m(\phi) + q_m \phi \quad (21)$$

The Laplacian operator  $\mathcal{L}_m$  for each azimuthal mode  $m$  is given by

$$\mathcal{L}_m(\phi) = \left[ \frac{1}{r} \frac{\partial}{\partial r} \left( r \frac{\partial \phi}{\partial r} \right) - \frac{m^2}{r^2} \right] \phi \quad (22)$$

and the function  $q_m$  is

$$q_m = \frac{m}{\varepsilon_0 r} \frac{\partial}{\partial r} \left( \frac{\rho}{B_z} \right) \quad (23)$$

For the electrospheric plasma, we can eliminate  $\rho$  by Eq. (14) and write

$$q_m = -\frac{m}{r} \frac{\partial}{\partial r} \left[ \frac{1}{r} \frac{\partial}{\partial r} (r^2 \Omega) + \frac{r\Omega}{B_z} \frac{\partial B_z}{\partial r} \right] \quad (24)$$

Note that this function does not depend on the intensity of  $B_z$  but only on its radial profile. However, it depends linearly on the amplitude of the differential rotation, meaning that strong departure from corotation leads to strong instability as will be shown in the next section. The eigenvalue problem Eq. (21) is supplemented by homogeneous boundary conditions such that the perturbed potential vanishes at the boundaries, namely

$$\phi(W_1) = \phi(W_2) = 0 \quad (25)$$

### 3.2. Multi-domain decomposition

When vacuum gaps exist between the walls and the plasma, the discontinuity in the density profile introduces a Gibbs phenomenon and therefore drastically decreases the efficiency of our pseudo-spectral algorithm. To overcome this difficulty, we decompose the space between the two walls into three distinct regions, namely

- region I: vacuum space between inner wall and inner boundary of the plasma column, the solution for the electric potential is denoted by  $\phi_I$ , defined for  $W_1 \leq r \leq R_1$  ;
- region II: the plasma column itself located between  $R_1$  and  $R_2$ , solution denoted by  $\phi_{II}$ , defined for  $R_1 \leq r \leq R_2$  ;
- region III: vacuum space between outer boundary of the plasma column and the outer wall, solution denoted by  $\phi_{III}$ , defined for  $R_2 \leq r \leq W_2$ .

In region I and III, the vacuum solutions which satisfy the required boundary conditions ( $\phi_I(W_1) = 0$  and  $\phi_{III}(W_2) = 0$ ) are given by the usual solutions to Laplace equation in the form

$$\phi_I(r) = A \left( r^m - \frac{W_1^{2m+1}}{r^{m+1}} \right) \quad (26)$$

$$\phi_{III}(r) = B \left( r^m - \frac{W_2^{2m+1}}{r^{m+1}} \right) \quad (27)$$

where  $A$  and  $B$  are two constants to be determined by matching the boundary conditions at the interfaces between plasma and vacuum. Because no surface charges accumulate on these interfaces (the equilibrium density profile should vanish at  $R_1$  and  $R_2$ ), the electric field is continuous in the whole space. The matching conditions are therefore, continuity of  $\phi$  and of its first derivatives, namely

$$\phi_I(R_1) = \phi_{II}(R_1) \quad (28)$$

$$\phi'_I(R_1) = \phi'_{II}(R_1) \quad (29)$$

$$\phi_{III}(R_2) = \phi_{II}(R_2) \quad (30)$$

$$\phi'_{III}(R_2) = \phi'_{II}(R_2) \quad (31)$$

We eliminate  $A$  and  $B$  from these equations to get the boundary conditions for  $\phi_{II}$ . We find that in the plasma column, the potential has to satisfy mixed boundary conditions of Robin type

$$\alpha_{1/2} \phi_{II}(R_{1/2}) + \beta_{1/2} \phi'_{II}(R_{1/2}) = 0 \quad (32)$$

with the coefficients given by

$$\alpha_{1/2} = \left( m R_{1/2}^{m-1} + (m+1) \frac{W_{1/2}^{2m+1}}{R_{1/2}^{m+2}} \right) \quad (33)$$

$$\beta_{1/2} = - \left( R_{1/2}^m - \frac{W_{1/2}^{2m+1}}{R_{1/2}^{m+1}} \right) \quad (34)$$

The boundary conditions Eq. (32) are the generalisation of the homogeneous Dirichlet case Eq. (25) when vacuum gaps are present. If the vacuum regions were removed such that  $W_1 = R_1$  and  $W_2 = R_2$ , the coefficients  $\beta_{1/2}$  in Eq. (32) would vanish whereas  $\alpha_{1/2} \neq 0$ . We therefore find again the homogeneous boundary conditions of the previous subsection, Eq. (25).

## 4. NUMERICAL PROCEDURE

### 4.1. Single domain

In the single domain decomposition, the plasma is in contact with both, the inner and outer wall. Thus  $W_1 = R_1$  and  $W_2 = R_2$ . There is no need to distinguish between  $R$  and  $W$ . The generalised linear eigenvalue problem Eq. (21) is solved numerically by using a pseudo-spectral Galerkin method

taking advantage of the homogeneous boundary conditions imposed on the perturbed electric potential,  $\phi(R_{1/2}) = 0$ . First, the independent variable  $r$  in Eq. (21) is transformed into a new independent variable  $x$  such that  $r \in [R_1, R_2]$  is mapped into the interval  $x \in [-1, 1]$ . This coordinate transformation reads :

$$r = \frac{R_2 - R_1}{2} x + \frac{R_2 + R_1}{2} \quad (35)$$

Second, the unknown eigenfunction  $\phi$  is expanded into a set of basis functions  $(\psi_k)_{k \geq 2}$  (Boyd 2001) defined for  $n \geq 1$  by :

$$\psi_{2n}(x) \equiv T_{2n}(x) - 1 \quad (36)$$

$$\psi_{2n+1}(x) \equiv T_{2n+1}(x) - x \quad (37)$$

Therefore the boundary conditions are automatically satisfied for each function of this particular basis,  $\psi_k(\pm 1)|_{k \geq 2} = 0$ . Here  $T_k(x) = \cos(k \arccos(x))$  are the Tchebyshev polynomials. Let  $N$  being the number of collocation points  $(x_i)_{0 \leq i \leq N-1}$  for the Tchebyshev expansion :

$$x_i = \cos\left(\frac{i \pi}{N-1}\right) \quad i = 0, 1, \dots, N-1 \quad (38)$$

The unknown function is expanded according to :

$$\phi(x) = \sum_{k=2}^{N-1} \phi_k \psi_k(x) \quad (39)$$

The matrix discretisation of Eq. (21) leads to the generalised linear eigenvalue problem

$$L \phi = \omega M \phi \quad (40)$$

where we have introduced the unknown vector  $\phi = (\phi_2, \phi_3, \dots, \phi_{N-1})$  and the square matrices are defined by :

$$L_{i-1, k-2} \equiv m \Omega(x_i) \mathcal{L}_m(\psi_k)(x_i) + q_m(x_i) \psi_k(x_i) \quad (41)$$

$$M_{i-1, k-2} \equiv \mathcal{L}_m(\psi_k)(x_i) \quad (42)$$

$$i = 1, 2, \dots, N-2$$

$$k = 2, 3, \dots, N-1$$

The system Eq. (40) is then solved by standard routines to compute the eigenvalues and the eigenvectors.

#### 4.2. Multi-domain decomposition

In the multi-domain decomposition, the Galerkin basis Eq. (36)-(37) is not adapted anymore. The new basis functions have to satisfy the following Robin boundary conditions :

$$\alpha_1 \psi_k(-1) + \beta_1 \psi'_k(-1) = 0 \quad (43)$$

$$\alpha_2 \psi_k(+1) + \beta_2 \psi'_k(+1) = 0 \quad (44)$$

We look for basis functions expressed by a three term expansion in Tchebyshev polynomials, for  $k \geq 2$ , like

$$\psi_k(x) = T_k(x) + a_k T_{k-1}(x) + b_k T_{k-2}(x) \quad (45)$$



For  $\psi_k(x)$  to satisfy the conditions Eq. (43)-(44), the unknowns  $a_k$  and  $b_k$  have to be solutions of the following system

$$a_k [\beta_1 (k-1)^2 - \alpha_1] + b_k [\alpha_1 - \beta_1 (k-2)^2] = -\alpha_1 + \beta_1 k^2 \quad (46)$$

$$a_k [\beta_2 (k-1)^2 + \alpha_2] + b_k [\alpha_2 + \beta_2 (k-2)^2] = -\alpha_2 - \beta_2 k^2 \quad (47)$$

The procedure to discretise the eigenvalue problem is the same as the one described in the previous section. We need only to replace the old basis Eq. (36)-(37) by the new basis Eq. (45).

## 5. RESULTS

Using the aforementioned numerical algorithm, we compute the eigenfunctions and eigenspectra of the diocotron instability for various equilibrium density profiles and charges on the inner wall for laboratory plasmas, Sec. 5.1 and several rotation profiles for pulsar’s electrosphere, Sec. 5.2.

In all computations, the external magnetic field follows a decreasing power law with index  $\alpha \geq 0$  such that

$$B_z = \frac{B_0}{r^\alpha} \quad (48)$$

### 5.1. Plasma column

First, we consider the laboratory plasma confined by some external experimental electromagnetic devices. The magnetic field and the density profile are specified as initial data. The rotation profile is then deduced from the electric drift approximation Eq. (17).

#### 5.1.1. Constant density profile

The simplest case corresponds to a uniform magnetic field  $B_0$ ,  $\alpha = 0$  and a constant charge density  $\rho_0$  extending from the origin  $r = 0$  to the outer wall, so  $W_1 = R_1 = 0$ , no inner conducting wall,  $W_2 = R_2$  and also  $Q = 0$  (single domain). In this particular case, the equilibrium speed is constant :

$$\Omega = -\frac{\rho_0}{2\varepsilon_0 B_0} \quad (49)$$

The functions  $q_m$  are all identically zero and the analytical solution to the eigenvalue problem Eq. (40) is simply :

$$\omega = m\Omega \quad (50)$$

There is no instability. Our numerical algorithm is able to reproduce the eigenvalues Eq. (50) with great accuracy taking only a few discretisation points (9 points are already enough). The convergence is very fast due to the evanescent truncation error introduced by the Tchebyshev expansion. The precision achieves easily 10 digits.

#### 5.1.2. Decreasing density profile

Next we consider a monotonely decreasing density profile starting from  $\rho_0$  at  $r = W_1 = R_1$  and vanishing at  $r = W_2 = R_2$  (single domain) such that

$$\rho = \rho_0 \frac{R_2^2 - r^2}{R_2^2 - R_1^2} \quad (51)$$

The corresponding rotation profile can be found analytically. The electric field induced by the plasma is deduced from Eq. (6) whereas the contribution from the wall is given by Eq. (2). Using the drift approximation Eq. (11), the total radial electric field expressed in Eq. (7) and the power law index for the magnetic field Eq. (48), the rotation speed of the plasma column in the most general case ( $\alpha$  and  $Q$  arbitrary) is equal to

$$\Omega = -\frac{\rho_0 r^\alpha}{\varepsilon_0 B_0 (R_2^2 - R_1^2)} \left[ \frac{R_2^2}{2} \left( 1 - \frac{R_1^2}{r^2} \right) - \frac{1}{4} \left( r^2 - \frac{R_1^4}{r^2} \right) \right] - \frac{Q}{2\pi \varepsilon_0 r^{2-\alpha} B_0} \quad (52)$$

When the plasma is in contact with the inner as well as with the outer conducting wall and the applied magnetic field is uniform, there is no diocotron instability, Briggs et al. (1970). Indeed, for  $\alpha = 0$ , all the eigenvalues we found are real as expected. For the first azimuthal modes  $m \leq 19$ , the map of the eigenvalues in the complex plane is shown in Fig. 1 for an uniform magnetic field,  $\alpha = 0$ , zero charge,  $Q = 0$ ,  $W_1 = R_1 = 1$  and  $W_2 = R_2 = 20$ . We normalised the frequencies to the rotation frequency  $\omega_r = \omega_p^2/4\omega_c = 1/400$ . Therefore, for each mode, the spectrum is continuous and delimited by two integer values, namely

$$0 \geq \omega_m/\omega_r \geq -2m \quad (53)$$

A similar conclusion applies also when the inner wall is removed ( $W_1 = R_1 = 0$ ), see Fig. 2. In this case the continuous spectra satisfy

$$-m \geq \omega_m/\omega_r \geq -2m \quad (54)$$

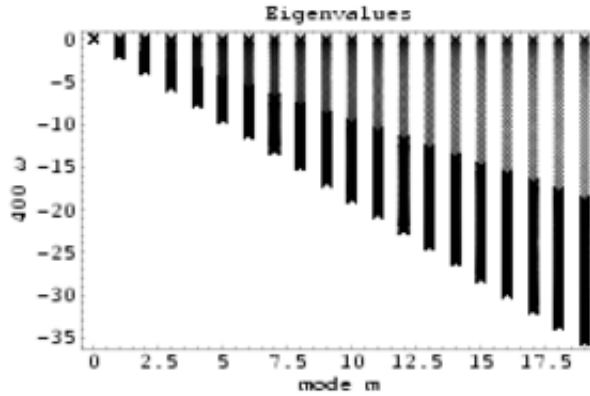


**Fig. 1.** Eigenvalues for the monotonely decreasing density profile Eq. (51). The boundaries are set to  $W_1 = R_1 = 1$  and  $W_2 = R_2 = 20$ . The other parameters are  $\alpha = 0$  and  $Q = 0$ . The continuous spectrum is shown for the azimuthal modes  $m = 0..19$ . The eigenfrequencies have been normalised to the rotation frequency  $\omega_r = \omega_p^2/4\omega_c = 1/400$ .

Finally when switching from an uniform magnetic field to a decreasing power law Eq. (48) with for instance  $\alpha = 1$ , the results are qualitatively unchanged, see Fig. 3. As can be seen by comparing the two maps on Fig. 1 and Fig. 3, the radial profile of the magnetic field does not influence much the eigenvalues. There is mainly a difference in scale because the rotation profile for  $\alpha = 1$  leads to higher rotation rate due to the extra factor  $r^\alpha$  in Eq. (52).

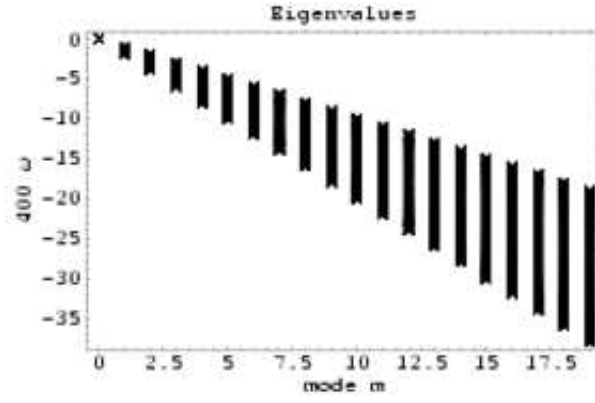


**Fig. 2.** Same as Fig. 1 but the inner wall has been removed, i.e.  $W_1 = R_1 = 0$ .

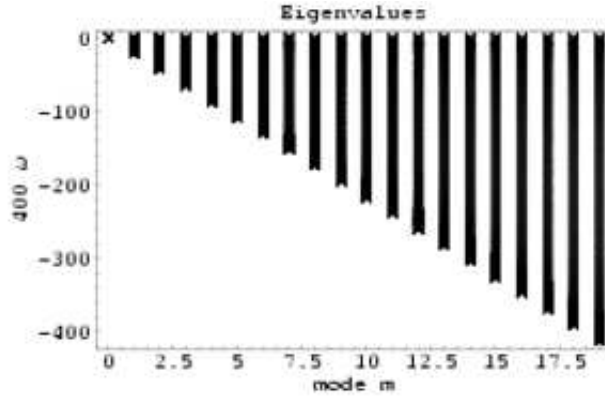


**Fig. 3.** Same as Fig. 1 but with a decreasing external magnetic field,  $\alpha = 1$ . Note the difference in scale for both cases.

### 5.1.3. Gaussian density profile

Next we consider a situation in which the plasma is not in contact with neither the inner nor the outer wall and so  $W_1 < R_1$  and  $W_2 > R_2$ , (multi-domain decomposition). We choose a Gaussian density profile given by

$$\rho = \rho_0 e^{-(r-a)^2/2\sigma^2} \quad (55)$$

$\sigma$  is a measure of the profile radial spread while  $a$  specifies the location of the centre of the plasma column. The associated rotation rate of the plasma column in the most general case ( $\alpha$  and  $Q$  arbitrary) is found analytically to be :

$$\Omega = -\frac{\rho_0 \sigma}{\epsilon_0 B_0 r^{2-\alpha}} \left[ \sigma \left\{ e^{-(R_1-a)^2/2\sigma^2} - e^{-(r-a)^2/2\sigma^2} \right\} + a \sqrt{\frac{\pi}{2}} \left\{ \operatorname{erf}\left(\frac{r-a}{\sigma \sqrt{2}}\right) - \operatorname{erf}\left(\frac{R_1-a}{\sigma \sqrt{2}}\right) \right\} \right] - \frac{Q}{2\pi \epsilon_0 r^{2-\alpha} B_0} \quad (56)$$

$\operatorname{erf}(x)$  is the error function, Abramowitz and Stegun (1965). In this case, we expect a strong diocotron instability with growth rates of the same order of magnitude as the rotation speed of the perturbation.

Indeed, taking boundaries such that  $W_1 = 1$ ,  $W_2 = 20$ ,  $R_1 = 5$  and  $R_2 = 10$  and an uniform magnetic field  $\alpha = 0$ , no charge on the inner wall  $Q = 0$ , the map of the eigenvalues in the complex plane is given by Fig. 4. Only the low azimuthal unstable modes are excited, from  $m = 1$

to  $m = 7$ , the fastest mode being  $m = 4$  with  $\gamma_{\max} \approx 1.15 \times 10^{-3}$  which is of the same order of magnitude as the real part,  $\text{Re}(\omega)/m$ . Removing the inner wall has little effect on the diocotron

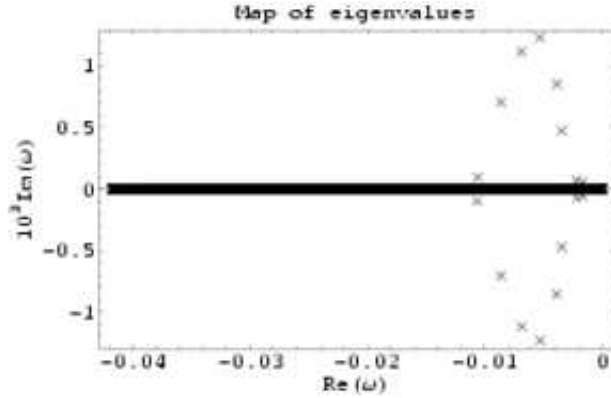


**Fig. 4.** Eigenvalues for the Gaussian density profile Eq. (55) with  $\sigma = 1$  and  $a = 7$ . The boundaries are set to  $W_1 = 1$ ,  $W_2 = 20$ ,  $R_1 = 5$ ,  $R_2 = 10$  and  $\alpha = 0$ .

spectrum, compare Fig. 4 and Fig. 5. Indeed, the instability is initiated by the presence of a hole in the middle of the plasma column. Placing or removing an inner wall cannot suppress or generate the instability in this configuration. It can at most affect the rate at which the instability grows. Also,

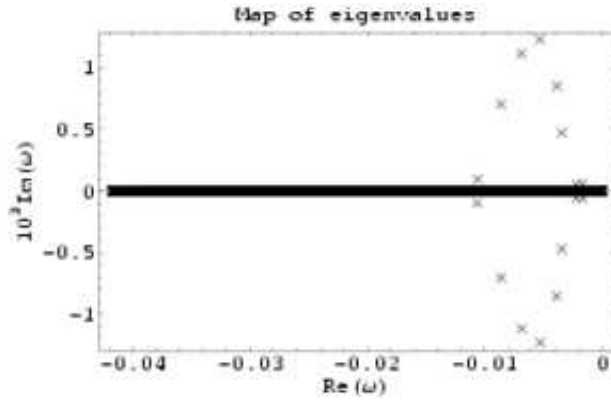


**Fig. 5.** Same as Fig. 4 but the inner wall has been removed, i.e.  $W_1 = 0$ .

a decreasing magnetic field  $\alpha = 1$  does not affect the results in a dramatic way, compare Fig. 4 and Fig. 6. The number of excited modes is directly related to the radial spread of the plasma column. More precisely, the thinner the plasma ring, the larger the number of unstable modes. In other words, decreasing  $\sigma$  will generate more unstable modes. In Fig. 7, we compare three Gaussian distributions with different spreads, namely  $\sigma = 1$ ,  $0.6$ ,  $0.4$ . The  $\sigma = 1$  profile has 7 unstable modes whereas the  $\sigma = 0.6$  profile has 10 unstable modes and the  $\sigma = 0.4$  profile 14. Meanwhile, the highest growth rate is also increasing significantly.

Finally, adding a charge to the inner wall does not affect drastically the map of eigenfrequencies, see Fig. 8. More unstable modes appear, nevertheless the maximum growth rates remain approximately in the same order of magnitude. Now that the algorithm has been checked and employed for different lab plasmas, we study in the next subsection the interesting case of an electrospheric plasma.

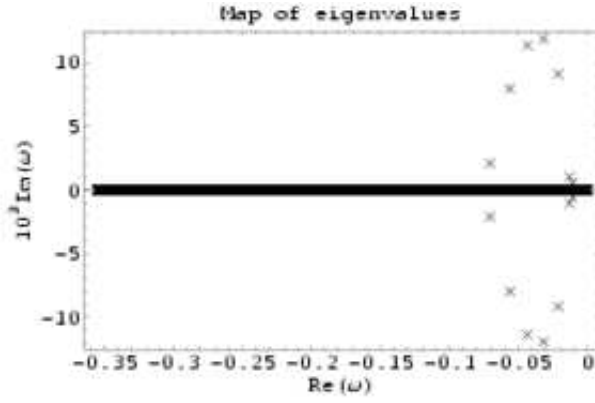


**Fig. 6.** Same as Fig. 4 but with a decreasing external magnetic field  $\alpha = 1$ .

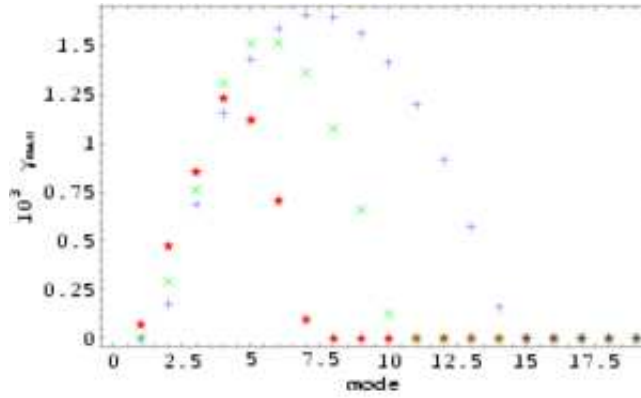


**Fig. 7.** Comparison of the highest growth rates for different spreads of the annular plasma column,  $\sigma = 1$  in red ‘stars’,  $\sigma = 0.6$  in green ‘x’ and  $\sigma = 0.4$  in blue ‘+’.

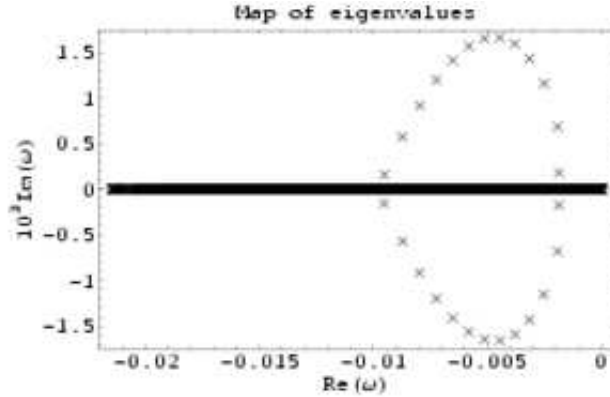


**Fig. 8.** Same as Fig. 4 but with a charge per unit length  $Q = 10$ .

## 5.2. Electrosphere

The electrospheric non-neutral plasma, as already proved in works by Krause-Polstorff and Michel (1985a) and Pétri et al. (2002a), is confined by the rotating magnetised neutron star. The most important feature is not the density profile but the rotation speed, although both are related in a unique manner, Eq. (14). Plasma shearing motion between different magnetic surfaces leads to a kind of Kelvin-Helmholtz instability, at least in the linear regime of the instability (the eigenvalue problems look very similar). (We always keep a single domain decomposition such that  $W_1 = R_1$

and  $W_2 = R_2$ ). Therefore, for electrospheric plasmas, we choose a rotation profile in the plasma column that mimics the rotation curve obtained in the 3D electrosphere. To study the influence of the profile, we took three different analytical expressions for the radial dependence of  $\Omega$  by mainly varying the gradient in differential shear as follows

$$\Omega(r) = 2 + \tanh[\alpha(r - r_0)] e^{-\beta r^4} \quad (57)$$

The values used are listed in Table (1).

| $\Omega$   | $\alpha$ | $\beta$            | $r_0$ |
|------------|----------|--------------------|-------|
| $\Omega_1$ | 3.0      | $5 \times 10^{-5}$ | 6.0   |
| $\Omega_2$ | 1.0      | $5 \times 10^{-5}$ | 6.0   |
| $\Omega_3$ | 0.3      | $5 \times 10^{-5}$ | 10.0  |

**Table 1.** Parameters for the three rotation profiles used to mimics the azimuthal velocity of the plasma in the electrospheric disk.

The angular velocity starts from corotation with the star  $\Omega = \Omega_* = 1$  (normalised to unity for convenience) followed by a sharp increase around  $r = 6$  for  $\Omega_{1,2}$  and a less pronounced gradient around  $r = 10$  for  $\Omega_3$ . Finally the rotation rate asymptotes twice the neutron star rotation speed, Fig. 9.

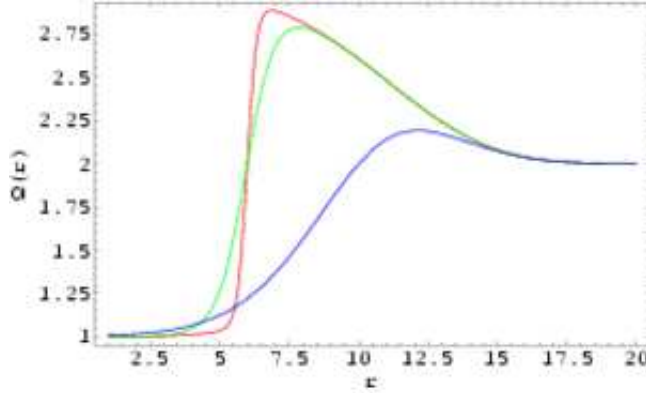


**Fig. 9.** Three choices of differential rotation curves in the plasma column for the cylindrical pulsar electrosphere,  $\Omega_1$  in red,  $\Omega_2$  in green and  $\Omega_3$  in blue.

### 5.2.1. Uniform magnetic field

First consider an uniform magnetic field,  $\alpha = 0$ . The maximum growth rates for the three rotation curves for each mode  $m$  are shown in Fig. 10.

The profile having the steepest gradient possesses the largest number of excited unstable modes because it corresponds to the case where the smallest scales appear, i.e.  $m$  large, red stars in Fig. 10. The largest growth rate, for  $m = 8$  its value is  $\gamma_{max} = 3.2$ , is even larger than the maximum rotation speed of the plasma column about  $\Omega_{max} = 2.9$ . The diocotron instability operates on a very short timescale, comparable to the period of the pulsar.

The second steepest profile possesses less unstable modes as we would expect due to the fact that only larger scale structures can emerge with this slope of the differential rotation, green ‘×’ in Fig. 10. The third smooth profile has only four unstable modes, blue ‘+’ in Fig. 10. We give

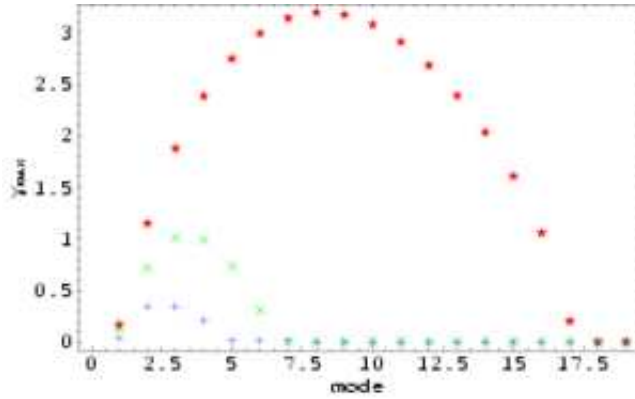


**Fig. 10.** Fastest growth rate  $\gamma_{max}$  for each azimuthal mode  $m$  and the three rotation profile shown in Fig. 9 in an uniform external magnetic field,  $\alpha = 0$ ,  $\Omega_1$  in red ‘stars’,  $\Omega_2$  in green ‘×’ and  $\Omega_3$  in blue ‘+’.

an example of eigenfunctions for the perturbed electric potential in Fig. 11. It corresponds to the fastest unstable mode for the profile  $\Omega_2$ . The boundary conditions impose  $\phi(R_{1/2}) = 0$  as seen on the plot. The corotation radius  $r_c$  defined by

$$\Omega(r_c) = \frac{Re(\omega)}{m} \quad (58)$$

is also shown on this plot, depicted by a vertical bar.

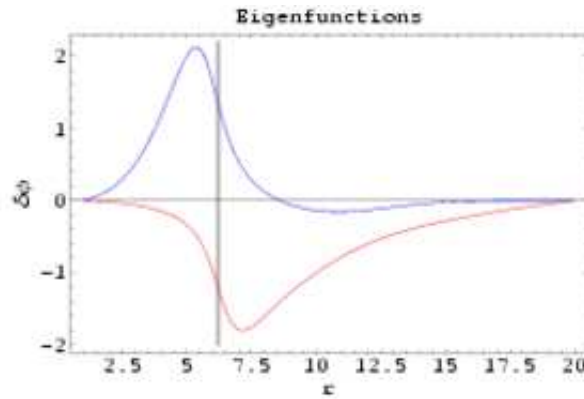


**Fig. 11.** Real (red curve) and imaginary (blue curve) part of the fastest growing eigenfunction for  $\Omega_2$  in an uniform magnetic field. The vertical bar shows the location of the corotation radius.

### 5.2.2. Dipolar magnetic field

Next consider a dipolar magnetic field,  $\alpha = 3$ . The maximum growth rates for the three rotation curves for each mode  $m$  are shown in Fig. 13.

We can draw the same conclusions as in the previous case. The largest number of excited unstable modes is observed for the steepest profile  $\Omega_3$ . Comparing Fig. 12 with Fig. 10, the value of the

maximum growth rate for each mode is not strongly affected by the geometry of the magnetic field. Here also, we give an example of eigenfunctions for the perturbed electric potential in Fig. 13. It

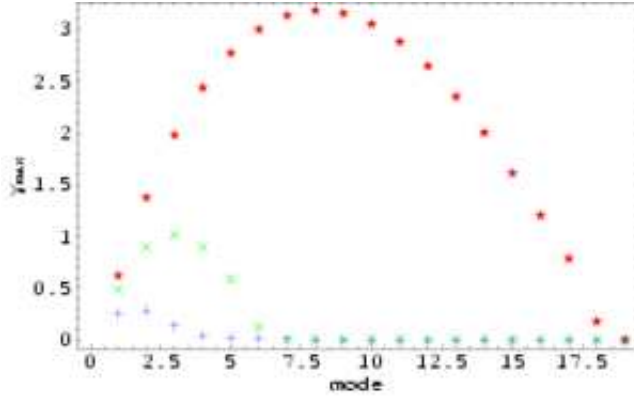


**Fig. 12.** Fastest growth rate  $\gamma_{max}$  for each azimuthal mode  $m$  and the three rotation profile shown in Fig. 9 in a dipolar external magnetic field,  $\alpha = 3$ ,  $\Omega_1$  in red ‘stars’,  $\Omega_2$  in green ‘x’ and  $\Omega_3$  in blue ‘+’.

corresponds again to the fastest unstable mode for the profile  $\Omega_2$ . The boundary conditions impose  $\phi(R_{1/2}) = 0$  as seen on the plot. Comparing Fig. 13 with Fig. 11, close to the inner boundary, the real part of the eigenfunctions look very similar. Nevertheless when approaching the outer boundary, the difference becomes appreciable because of the strong departure from an uniform magnetic field.

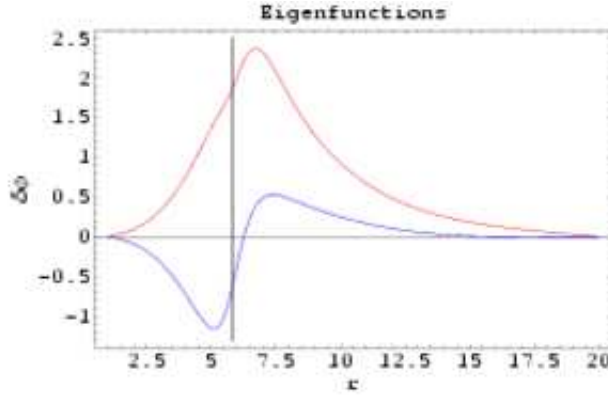


**Fig. 13.** Real (red curve) and imaginary (blue curve) part of the fastest growing eigenfunction for  $\Omega_2$  in an dipolar magnetic field. The vertical bar shows the location of the corotation radius.

## 6. CONCLUSION

We developed a pseudo-spectral Galerkin code to compute the eigenspectra and eigenfunctions of the diocotron instability for arbitrary magnetic field configurations and density profiles. The code is very efficient in computing the fastest growing modes. When increasing the number of points, convergence is reached quickly, in most cases, less than 200 points are needed. Application to the pulsar shows that the diocotron regime gives rise to instabilities with growth rate comparable to



the rotation period of the neutron star. This confirms the results of our previous work (Pétri et al 2002b) and shows that the precise geometry, let it be a flat disk or a column of plasma, does not affect drastically the diocotron instability. The required ingredients are only non-neutral plasmas and shear velocities.

In a forthcoming paper, we plan to investigate the full non-linear development of the diocotron instability by means of 2D electrostatic PIC simulations. We will also add an external source of charge feeding the system and demonstrate that particle transport across the magnetic field line is possible. Note that this has already been observed in some experiments by Pasquini and Fajans (2002).

Extension to plasma moving with relativistic speeds is also envisageable, in particular the generalisation to the electromagnetic non-neutral instability regime, the so-called magnetron instability. Last but not least, the influence of finite temperature in the plasma on the diocotron instability would require a kinetic treatment of the stability via the Vlasov-Maxwell equation.

*Acknowledgements.* I am grateful to Jean Heyvaerts for his helpful comments and suggestions. This work was supported by a grant from the G.I.F., the German-Israeli Foundation for Scientific Research and Development.

## References

- Abramowitz, M. and Stegun, I. A. *Handbook of mathematical functions*, New York: Dover, 1965
- Aly, J. J. 2005, A&A, 434, 405
- Bhattacharyya, S. N. 2000, *Physics of Plasmas*, 7, 4805
- Boyd, J. P. 2001, *Chebyshev and Fourier Spectral Methods*, Springer-Verlag
- Briggs, R. J., Daugherty, J. D. and Levy, R. H. 1970, *Physics of Fluids*, 13, 2, 421
- Davidson, R. C. and Tsang, K. 1984 *Phys. Rev. A*, 30, 488
- Davidson, R. C. 1990, *Physics of non neutral plasmas*, Addison-Wesley Publishing Company
- Goswami, P., Bhattacharyya, S. N., Sen, A., and Maheshwari K. P. 1999, *Physics of Plasmas*, 6, 3442
- Krause-Polstorff, J. and Michel, F. C. 1985a, MNRAS, 213, 43P
- Krause-Polstorff, J. and Michel, F. C. 1985b, A&A, 144, 72
- Levy, R.H. 1965, *Physics of Fluids*, 8, 1288
- Michel, F. C. 2005, *Revista Mexicana de Astronomia y Astrofisica Conference Series*, 27
- Neukirch, T. 1993, A&A, 274, 319
- O’Neil, T. M. 1980, *Physics of Fluids*, 23, 2216
- O’Neil, T. M. and Smith, R. A. 1992, *Physics of Fluids B*, 4, 2720
- Pasquini, T. and Fajans, J. 2002, AIP Conf. Proc. 606: Non-Neutral Plasma Physics IV, 453
- Pétri, J., Heyvaerts, J. and Bonazzola, S. 2002a, A&A, 384, 414
- Pétri, J., Heyvaerts, J. and Bonazzola, S. 2002b, A&A, 387, 520
- Pétri, J., Heyvaerts, J. and Bonazzola, S. 2003, A&A, 411, 203
- Rylov, I. A. 1989, Ap&SS, 158, 297
- Shibata, S. 1989, Ap&SS, 161, 187
- Smith, I. A., Michel, F. C., and Thacker, P. D. 2001, MNRAS, 322, 209
- Spitkovsky, A. and Arons, J. 2002, ASP Conf. Ser. 271: Neutron Stars in Supernova Remnants, 81
- Thielheim, K. O. and Wolfstetter, H. 1994, ApJ, 431, 718
- Zachariades, H. A. 1993, A&A, 268, 705